

High contrast imaging and thickness determination of graphene with in-column secondary electron microscopy

Vidya Kochat,¹ Atindra Nath Pal,¹ Sneha E. S.,¹ Arjun B. S.,² Anshita Gairola,² S. A. Shivashankar,² Srinivasan Raghavan,² and Arindam Ghosh¹
¹ *Department of Physics, Indian Institute of Science, Bangalore 560 012, India and*
² *Materials Research Center, Indian Institute of Science, Bangalore 560 012, India*

We report a new method for quantitative estimation of graphene layer thicknesses using high contrast imaging of graphene films on insulating substrates with a scanning electron microscope. By detecting the attenuation of secondary electrons emitted from the substrate with an in-column low-energy electron detector, we have achieved very high thickness-dependent contrast that allows quantitative estimation of thickness up to several graphene layers. The nanometer scale spatial resolution of the electron micrographs also allows a simple structural characterization scheme for graphene, which has been applied to identify faults, wrinkles, voids, and patches of multilayer growth in large-area chemical vapor deposited graphene. We have discussed the factors, such as differential surface charging and electron beam induced current, that affect the contrast of graphene images in detail.

I. INTRODUCTION

As a two dimensional crystal of carbon atoms, graphene has attracted wide attention due to its potential applications in the field of ultra-fast electronics, sensing and photovoltaics, apart from providing a testing bed of the new and exotic physical phenomena. It has been observed that the electrical^{1,2}, thermal³, mechanical⁴ and optical⁵ properties of graphene films depend strongly on the number of graphene layers, because the band structure of multilayer graphene systems differs radically from monolayer graphene due to the interlayer coupling⁶. The number of layers determines the response of graphene to external factors too, such as its coupling to underlying substrates, disorder and adsorbates⁷⁻⁹. Hence with advances in new techniques for growing graphene at a macroscopic scale, which includes epitaxial growth on SiC¹⁰ or chemical vapor deposition on transition metals (copper, nickel, tungsten etc.)^{11,12}, there is a growing emphasis on a close monitoring of graphene thickness in a rapid and non-invasive manner with nanometer scale spatial resolution. In this letter we show that scanning electron microscopy (SEM) with an in-column secondary electron (SE) detector is an excellent tool for high-contrast layer-sensitive imaging of graphene, which is simple and overcomes many of the drawbacks of commonly used methods.

Several techniques have been used to characterize the thickness of graphene layers. This includes optical microscopy^{5,13}, atomic force microscopy (AFM)¹⁴, Raman spectroscopy¹⁵⁻¹⁷, contrast spectroscopy¹⁸, Rayleigh imaging¹⁹, low energy electron diffraction, angle-resolved ultraviolet photoemission spectroscopy²⁰ and Auger electron spectroscopy²¹. Optical microscopy is limited to identifying graphene layers on ~ 300 nm SiO₂. Raman spectroscopy is presently the most common technique used to distinguish between monolayer and bilayer graphene on SiO₂, but not regularly on other substrates like SiC, glass, Cu, Ni due to strong electronic cou-

pling between graphene and the substrate. Moreover, the diffraction limit of light imposes a restriction on the spatial resolution of Raman spectroscopy of graphene, as also in the cases of contrast spectroscopy and Rayleigh imaging. AFM is a direct technique to count the number of layers in graphene, even in sub-micron samples, but the tip-sample interaction¹⁴ and the topology of the substrate need to be carefully considered.

Recently, attenuation of low-energy electrons in graphene has been exploited in Auger electron spectroscopy (AES) to determine the number of graphene layers²¹. The energy relaxation of incident electrons on graphene occurs over the inelastic mean free path ($\lambda \approx 0.45$ nm below 100 eV), thereby modulating the intensity with varying thickness in the AES electron maps. Although it is recognized that such a process can yield high contrast images of multilayer graphene in

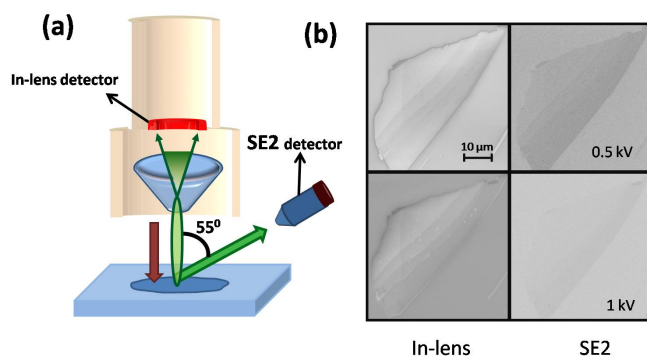


FIG. 1: (a) Schematic of secondary electron detection by the in-lens detector placed inside the electron column and the Everhart - Thornley detector (ETD) placed outside the column at an angle of 55°. (b) The difference in contrast between the images taken by the in-lens detector and the ETD are shown for a typical multilayer graphene sample at two primary electron energies.

SEM as well²², a quantitative understanding of attenuation of low-energy SE by graphene in an SEM is still lacking. Experiments using an outer SE detector (often an Everhart-Thornley detector) generally yield relatively poor contrast, making a quantitative analysis less reliable. Instead, an in-column SE detector (in-lens) in a field-emission SEM (FESEM), which generally responds to lower electron energies (\sim few tens of eV), has been known to produce images of very sharp contrast for carbon nanotubes on insulating substrates^{23,24}. Since it is assumed that the interaction between the SE emitted from the substrate and the nanotube is negligible, the physical mechanism behind this contrast is under debate, and both voltage contrast due to differential surface charging²³ and electron beam induced current (EBIC) processes²⁴ have been suggested. Here we show that low-energy SE imaging using the in-lens detector of a FESEM provides a sharp thickness-dependent contrast of graphene on insulating substrates over a wide range of primary electron energies, E_p . We present a quantitative analysis of the thickness determination of graphene by taking into account the attenuation of SE of the substrate by the graphene layers. Due to inherent spatial resolution of SEM (typically $\lesssim 2$ nm at $E_p = 5$ kV), this technique can be extremely useful in examining nanostructures of graphene, such as graphene nanoribbons, and also in detecting folds, discontinuities and multi-layer growth in large area graphene.

II. EXPERIMENTAL DETAILS

We have carried out detailed SEM studies on two types of graphene in this work, namely exfoliated and chemical vapor deposited (CVD) graphene. Exfoliated graphene flakes were prepared by micromechanical exfoliation of natural graphite on n^{++} doped silicon substrate covered with 300 nm thick SiO_2 on top. The CVD-graphene was grown by thermal decomposition of methane on copper at 1000°C. The graphene was transferred onto the substrate by coating the copper foil with Poly(methyl methacrylate) (PMMA 950K), after which the copper was etched off by placing the foil in an etch solution of Ferric Chloride. The graphene/PMMA film was then transferred on to the substrate which was then rinsed in acetone, to dissolve the PMMA leaving graphene on the substrate. The graphene films were characterized by Raman spectroscopy and AFM to identify the number of layers in various regions. The SEM images of the graphene films were obtained using an in-lens detector placed inside the electron column of a Carl Zeiss Σ IGMA FESEM, and also an Everhart-Thornley detector (SE2) placed outside the column at an angle of 55° from the column axis. The arrangement is schematically shown in Fig. 1a. When the primary electron beam is incident on the sample, low-energy SE and high-energy backscattered electrons (BSE) are produced from the substrate in the vicinity of the beam exposed region. The SE and BSE are attracted

by the positively biased beam booster of the electron column and are projected towards the in-lens detector. The BSE are generated from deep within the substrate and pass through the central aperture of the in-lens detector without being collected. The in-lens detector collects low-energy SE efficiently while the SE2 collects high energy SE that are not collected by the in-lens detector. For preliminary comparison, in Fig. 1b we show a typical multilayer exfoliated graphene flake containing 2 – 6 layers (see optical image in Fig. 2a) on SiO_2 substrate for two values of $E_p = 0.5$ kV and 1 kV. In both cases the in-lens image has better contrast, giving graphene greater visibility on SiO_2 substrate, than the SE2 image. This indicates that graphene interacts mainly with low-energy SE, and becomes progressively transparent to high-energy SE which are collected at SE2.

Given this observation, graphene films were subsequently imaged with the in-lens detector at varying E_p ranging from 0.5 - 10 kV at a working distance of 5 mm. The beam current used for the imaging was kept low, in the range of 9 - 16 pA in this voltage regime, in order to reduce the electron beam induced damage to graphene^{25–27}. Strikingly, we find the image contrast to vary strongly with changing E_p as seen from Fig. 2a, and regions having different thicknesses can be identified from discrete shifts in intensity. The thickness of graphene layers in various regions of the film has been labeled in the optical micrograph. Note that the overall contrast as well as that of individual layers is best around $E_p \simeq 3$ kV, which is similar to that observed in case of carbon nanotubes on SiO_2 (around 1 kV)^{23,24}, thereby indicating that this is due to the nature of the substrate. This optimum value of $E_p \approx 3$ kV for graphene imaging is an important result.

III. RESULTS AND DISCUSSION

A. Voltage contrast imaging of graphene layers

This contrast mechanism can be understood by considering the low ($\lesssim 1$ kV), the intermediate ($1\text{ kV} \leq E_p \leq 3\text{ kV}$) and high ($\gtrsim 5$ kV) regimes of E_p separately. When $E_p \sim 1$ kV, the number of SE emitted from SiO_2 surface becomes more than the number of incident electrons which leads to a depletion of electrons from the SiO_2 surface. Consequently, the SiO_2 surface becomes positively charged which results in a flow of EBIC from graphene to SiO_2 surface replenishing that region with electrons and increasing the SE emission from the SiO_2 region beneath graphene. This results in negative contrast for $E_p \leq 1$ kV. Further we observed that increasing the beam current while reducing the scan time (or equivalently increasing the scan rate) increases the contrast. In this situation the time taken for SE signal acquisition from a pixel in the substrate is reduced, allowing less time for charge dissipation in the substrate during the SE signal collection, and hence greater pixel-time aver-

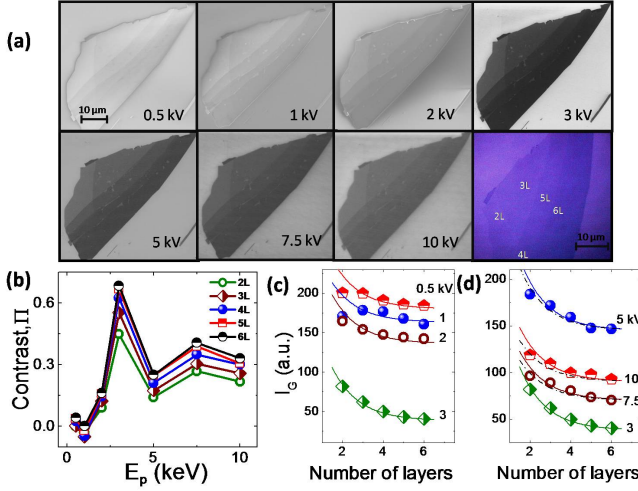


FIG. 2: (a) In-lens images for graphene film with 2 - 6 layers acquired with a scan rate of $7.2 \mu\text{m/s}$ for acceleration voltages from 0.5 - 10 kV. The last panel shows an optical micrograph identifying different layers. (b) The contrast parameter (Eq.1) for various layers is plotted as a function of incident beam energy. The contrast between the different graphene layers and SiO_2 substrate is maximum at 3kV. (c),(d) The absolute intensity (I_G) of SE emission from different graphene layers as a function of number of graphene layers for primary electron energy $\leq 3\text{kV}$ (c) and $\geq 3\text{kV}$ (d). The solid curves denote the fit using Eq.2 with $\alpha = 1$ and the dashed curves represent I_{sub} multiplied by a fraction which takes into account the negative charging of graphene.

aged local potential difference giving greater EBIC and SE signal.

The positive charging of the substrate reduces in the intermediate kV regime (1.5 - 3 kV), due to which the EBIC from graphene to SiO_2 also reduces. Around 3kV, the EBIC is a minimum due to minimal surface charging and the emitted SE are simply attenuated by graphene layers giving rise to a contrast reversal at 3kV. At very high kV ($\geq 5\text{kV}$), a large number of SE are produced in the bulk of SiO_2 and Si. But since the SE are produced from depths which are large compared to their escape depth, the number of SE emitted are less leading to negative charging of the substrate. The graphene layers also get charged negatively due to negligible flow of EBIC to SiO_2 . The thinner regions of graphene which are less metallic, cannot dissipate charge easily and hence a surface negative potential gradient develops in the graphene region leading to greater suppression of SE emission from these regions. These combined effects lead to a reduction in contrast at very high kV.

B. Thickness determination of graphene layers

For quantitative analysis, we define the contrast parameter (Π) as,

$$\Pi = \frac{I_{sub} - I_G}{I_{sub} + I_G} \quad (1)$$

where I_G and I_{sub} are the local intensities at the graphene region and surrounding substrate (far away from graphene), respectively, which are proportional to the corresponding number of secondary electrons collected by the in-lens detector. As shown in Fig. 2b, Π varies similarly for all layer numbers and can be as large 0.7 at $E_p \approx 3\text{kV}$. In the discrete shifts in contrast (i.e. I_G) with increasing layer number (Fig. 2a), the thicker regions of graphene always appear darker than the thinner regions, which implies I_G decreases with increasing layer number for fixed values of E_p , as shown in Fig. 2c ($E_p \leq 3\text{kV}$) and Fig. 2d ($E_p \geq 3\text{kV}$). We attribute this to attenuation of the SE within multilayer graphene which can be quantitatively expressed as²¹,

$$I_G(N) = \alpha I_{sub} \exp \left[-\frac{(N-1)d_0 + d_{vdw}}{\lambda} \right] + I_0 \quad (2)$$

where N , d_0 ($= 0.335\text{ nm}$), and d_{vdw} ($\approx 0.35\text{ nm}$) are the number of layers, inter-layer separation in graphene, and the van der Waal distance of the graphene from SiO_2 substrate, respectively. The factor α accounts for the negative charging of graphene during electron beam scanning. All solid lines in Figs. 2c and 2d were obtained with $\alpha = 1$, $\lambda = 0.445\text{ nm}$ from AES data, and background intensity I_0 from the uncovered parts of SiO_2 . I_0 is the only fitting parameter in Eq. 2. The overall agreement of Eq. 2 to the observed data confirms SE attenuation by the graphene layers, and forms a new method to obtain the thickness of graphene with SEM. We note two extreme cases: (1) For $E_p \gtrsim 5\text{kV}$, $\alpha \approx 0.9$ gives a marginally better fit (dashed lines in Fig. 2d), which is due to slight negative charging of graphene which leads to the suppression of SE emission from the underneath substrate. (2) Secondly, at very low $E_p \lesssim 1\text{kV}$ (Fig. 2c), the SiO_2 surface beneath the thinner regions of graphene, which are less metallic, get significantly positively charged. This reduces I_G from these regions below the expectation of Eq. 2.

C. Contrast reversal in single layer graphene

The in-lens SEM imaging of single layer graphene (SLG) was found to display very different behavior with respect to acceleration voltage. Here we have examined three different classes of SLG devices: (1) Exfoliated SLG on SiO_2 substrate, (2) large-area CVD grown graphene on SiO_2 substrate, and (3) CVD graphene on high- k TiO_x substrate. We first focus on the in-lens images of exfoliated and CVD-grown SLG on SiO_2 substrate shown in Fig.3a and 3b, respectively. In the exfoliated case (Fig. 3a) we find that the graphene region appears brighter than the surrounding SiO_2 at all E_p . This leads to a *negative* contrast parameter Π (see Eq. 1), as opposed to the case of multilayer graphene where Π is positive (Fig. 2b). Π is most negative at small E_p , becomes

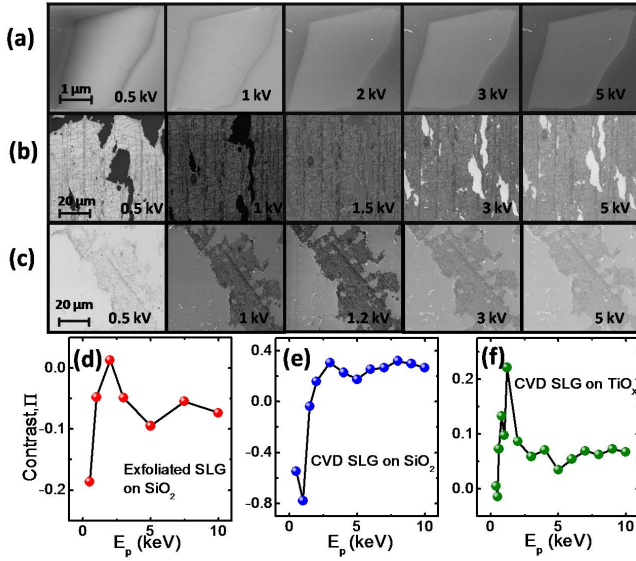


FIG. 3: (a) In-lens images of exfoliated single layer graphene on SiO_2/Si substrate for different primary electron energies. (b) In-lens images of CVD grown single layer graphene on SiO_2/Si substrate for different primary electron energies showing a sharp contrast reversal below 1kV. Due to a small drift at different acceleration voltages, the regions are slightly shifted downwards at higher acceleration voltages. (c) In-lens images of CVD grown single layer graphene on TiO_x/Si substrate for different primary energies which do not show a contrast reversal. All the SEM images in (a) - (c) were acquired in a scan time of 10.4 s. (d - f) Contrast as a function of primary energy for exfoliated SLG on SiO_2 , CVD grown SLG on SiO_2 and CVD grown SLG on TiO_x respectively.

nearly zero at $E_p \sim 2$ kV, but eventually settles to a small negative magnitude (~ -0.07) at large E_p (Fig. 3d). If we ignore the interaction of SLG with SE, the brightness of graphene images at low E_p can be explained in a manner similar to the case of carbon nanotubes^{23,24}. In this regime ($E_p < 2$ kV) differential surface charging due to the flow of EBIC from graphene to SiO_2 which results in an enhanced SE emission from the graphene-covered region of the substrate making it appear brighter. The consistency of this scenario could be readily verified by replacing SiO_2 with atomic layer deposited 350 nm of TiO_x which is a high- k dielectric with dielectric constant nearly 200. The surface charge is now heavily screened which reduces the EBIC, and hence, CVD-grown graphene on TiO_x substrate always appears darker at all values of E_p (Fig. 3c) with a maximum contrast at $E_p \approx 1.2$ kV. At higher E_p ($> 2 - 3$ kV), SLG becomes negatively charged when scanned by the electron beam. The contrast, whether positive or negative, is determined by the rate at which charge is dissipated from graphene to the substrate, in comparison to the rate at which graphene gets charged by the primary electron beam. A potential equilibrium is achieved more rapidly in the case of exfoliated SLG than the large area CVD graphene since

the scan time was kept constant during image acquisition. This explains why Π is negative for exfoliated SLG at large E_p , and for CVD graphene on SiO_2 and TiO_x substrates it saturates at a small positive value (Fig. 3e). Nonetheless, the reversal of contrast in in-lens SEM as a function of acceleration voltage can serve to separate the SLG from the multilayer graphene devices.

D. Applications

The high-contrast imaging of graphene layers at low kV can be an effective nondestructive and quick imaging tool for the structural characterization of voids, ruptures and folds on graphene at nanometer scale. This is particularly important in large area graphene, for example those grown by CVD and subsequently transferred onto a different (insulating) substrate. In Fig. 4a we demonstrate this with an SEM image of CVD-grown (on Cu) graphene transferred on to SiO_2 substrate ($E_p = 3$ kV). The wrinkles on CVD graphene observed as branched quasi-linear striations in Fig. 4a possibly represent the texture of the metal on which graphene was grown. The voids and ruptures which occurred during the transfer process are also easily visible. Additionally, randomly scattered darker patches seem to represent regions of multilayer growth. The multilayered regions are indicated in the intensity profile (inset of Fig. 4d) along the line shown in Fig. 4a. Eq. 2 provides a good fit to the intensity as a function of

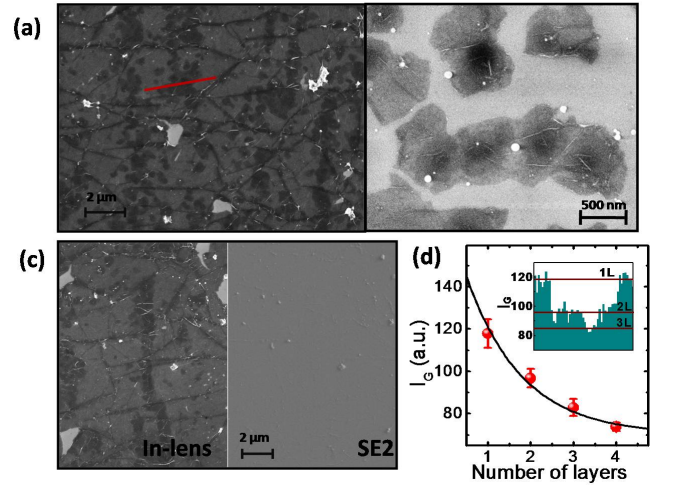


FIG. 4: (a) SEM In-lens image of ruptures, folds and regions of multilayer growth in large area graphene grown by chemical vapour deposition on copper and subsequently transferred onto SiO_2 substrate. (b) High resolution in-lens image of coalesced sub- μm sized graphene grains on SiO_2 showing excellent contrast. (c) A region of CVD graphene on SiO_2 imaged at a primary energy of 3kV using the in-lens detector and the outer detector. (d) The SE intensity of the various multilayer regions in the CVD graphene shown in (a) is fitted by eq.2. The inset shows the SE intensity along a line shown in the (a).

layer number (Fig. 4d), albeit with $\alpha \approx 0.5$ due to significant negative charging of the large area CVD graphene. Fig. 4b shows a high resolution in-lens image of nanometer sized graphene flakes grown by CVD acquired at a very fast scan rate of $450\mu\text{m/s}$, showing excellent contrast even at very large magnification. Finally, in Fig. 4c, a comparison of 3 kV in-lens and SE2 images are shown for a particular region of CVD graphene. It is clear that the SE2 imaging cannot capture the richness of structure on graphene provided by the in-lens, which is in agreement with the exfoliated case shown in Fig. 1b.

IV. CONCLUSIONS

In summary, we find that SEM imaging using an in-column secondary electron detector provides a very effi-

cient method of determination of thickness of graphene films on different insulating substrates. The contrast arises due to attenuation of secondary electrons from the underlying substrate by multilayer graphene, characterized by an inelastic mean free path. Differential charging of the substrate due to EBIC affects the contrast at low primary electron energies, and causes a “contrast reversal” phenomenon in single layer graphene on SiO_2 . We have also demonstrated that this technique can be exploited for structural characterization of graphene down to nanometer length scales.

Acknowledgment

We acknowledge the Department of Science and Technology (DST) for a funded project. S.R. acknowledges support under Grant No. SR/S2/CMP-02/2007. V.K. and A.N.P. thank CSIR for financial support.

-
- ¹ J. B. Oostinga, H. B. Heersche, X. Liu, A. F. Morpurgo and L. M. K. Vandersypen, *Nature Mater.* **7**, 151 (2007).
 - ² M. F. Craciun, S. Russo, M. Yamamoto, J. B. Oostinga, A. F. Morpurgo and S. Tarucha, *Nature Nanotech.* **4**, 383 (2009).
 - ³ S. Ghosh, W. Bao, D. L. Nika, S. Subrina, E. P. Pokatilov, C. N. Lau and A. A. Balandin, *Nat. Mater.* **9**, 555 (2010).
 - ⁴ I. W. Frank, D. M. Tanenbaum, A. M. van der Zande and P. L. McEuen, *J. Vac. Sci. Technol. B* **25**, 2558 (2007).
 - ⁵ P. Blake, K. S. Novoselov, A. H. Castro Neto, D. Jiang, R. Yang, T. J. Booth, A. K. Geim and E. W. Hill, *Appl. Phys. Lett.* **91**, 063124 (2007).
 - ⁶ E. McCann, *Phys. Rev. B* **74**, 161403(R) (2006).
 - ⁷ A. N. Pal and A. Ghosh, *Appl. Phys. Lett.* **95**, 082105 (2009).
 - ⁸ A. N. Pal and A. Ghosh, *Phys. Rev. Lett.* **102**, 126805 (2009).
 - ⁹ A. N. Pal, S. Ghatak, V. Kochat, E. S. Sneha, B. S. Arjun, S. Raghavan and A. Ghosh, *e-print arXiv:condmat/1009.5832v2* (2010).
 - ¹⁰ C. Berger, Z. Song, X. Li, X. Wu, N. Brown, C. Naud, D. Mayou, T. Li, J. Hass, A. N. Marchenkov, E. H. Conrad, P. N. First and W. A. de Heer, *Science* **312**, 1191 (2006).
 - ¹¹ X. Li, W. Cai, J. An, S. Kim, J. Nah, D. Yang, R. Piner, A. Velamakanni, I. Jung, E. Tutuc, S. K. Banerjee, L. Colombo and R. S. Ruoff, *Science* **324**, 1312 (2009).
 - ¹² A. Reina, X. Jia, J. Ho, D. Nezich, H. Son, V. Bulovic, M. S. Dresselhaus and J. Kong, *Nano Lett.* **9**, 30 (2009).
 - ¹³ P. E. Gaskell, H. S. Skulason, C. Rodenchuk and T. Szkopek, *Appl. Phys. Lett.* **94**, 143101 (2009).
 - ¹⁴ P. Nemes-Incze, Z. Osvtha, K. Kamarsb and L. P. Bira, *Carbon* **46**, 1435 (2008).
 - ¹⁵ A. C. Ferrari, J. C. Meyer, V. Scardaci, C. Casiraghi, M. Lazzeri, F. Mauri, S. Piscanec, D. Jiang, K. S. Novoselov, S. Roth and A. K. Geim, *Phys. Rev. Lett.* **97**, 187401 (2006).
 - ¹⁶ A. Das, S. Pisana, B. Chakraborty, S. Piscanec, S. K. Saha, U. V. Waghmare, K. S. Novoselov, H. R. Krishnamurthy, A. K. Geim, A. C. Ferrari and A. K. Sood, *Nature Nanotech.* **3**, 210 (2008).
 - ¹⁷ N. Camara, J.-R. Huntzinger, G. Rius, A. Tiberj, N. Mestres, F. Prez-Murano, P. Godignon and J. Camassel, *Phys. Rev. B* **80**, 125410 (2009).
 - ¹⁸ Z. H. Ni, H. M. Wang, J. Kasim, H. M. Fan, T. Yu, Y. H. Wu, Y. P. Feng and Z. X. Shen, *Nano Lett.* **7**, 2758 (2007).
 - ¹⁹ C. Casiraghi, A. Hartschuh, E. Lidorikis, H. Qian, H. Harutyunyan, T. Gokus, K. S. Novoselov and A. C. Ferrari, *Nano Lett.* **7**, 2711 (2007).
 - ²⁰ C. Riedl, A. A. Zakharov and U. Starke, *Appl. Phys. Lett.* **93**, 033106 (2008).
 - ²¹ M. Xu, D. Fujita, J. Gao and N. Hanagata, *ACS Nano* **4**, 2937 (2010).
 - ²² H. Hiura, H. Miyazaki and K. Tsukagoshi, *Appl. Phys. Exp.* **3**, 095101 (2010).
 - ²³ T. Brintlinger, Y.-F. Chen, T. Drkop, E. Cobas, M. S. Fuhrer, J. D. Barry and J. Melngailis, *Appl. Phys. Lett.* **81**, 2454 (2002).
 - ²⁴ Y. Homma, S. Suzuki, Y. Kobayashi, M. Nagase and D. Takagi, *Appl. Phys. Lett.* **84**, 1750 (2004).
 - ²⁵ G. Rius, A. Verdager, F. A. Chaves, I. Martn, P. Godignon, E. Lora-Tamayo, D. Jimnez and F. Prez-Murano, *Microelectron. Eng.* **85**, 1413 (2008).
 - ²⁶ D. Teweldebrhan and A. A. Balandin, *Appl. Phys. Lett.* **94**, 013101 (2009).
 - ²⁷ I. Childres, L. A. Jauregui, M. Foxe, J. Tian, R. Jalilian, I. Jovanovic and Y. P. Chen, *Appl. Phys. Lett.* **97**, 173109 (2010).